Neutron and synchrotron diffraction study of UPtGe

D. Mannix,* S. Coad, G. H. Lander, and J. Rebizant
European Commission, Joint Research Centre, Institute for Transuranium Elements, Postfach 2340, D-76125 Karlsruhe, Germany

P. J. Brown
Institut Laue Langevin, B.P. 156X, F-38042 Grenoble, France

J. A. Paixão
Department of Physics, University of Coimbra, P-3000 Coimbra, Portugal

S. Langridge†
European Synchrotron Radiation Facility, B.P. 220X, F-38043 Grenoble, France

S. Kawamata
College of Engineering, Osaka Prefecture University, Sakai 593, Japan

Y. Yamaguchi
Institute for Materials Research, Tohoku University, Sendai 980-77, Japan
(Received 6 March 2000)

UPtGe has an incommensurate and noncollinear magnetic structure. Neutron experiments on a single crystal have shown that the crystal structure is neither the TiNiSi nor disordered $CeCu_2$ type, as previously suggested, but rather the noncentrosymmetric EuAuGe structure, with two independent uranium atoms in the asymmetric unit. We report details of the cycloidal magnetic structure as examined by a conventional diffractometer, and the neutron polarimeter at the Institut Laue Langevin. The uranium moments are different on the two sites, with the average value of $1.4\mu_B$. A single magnetic domain exists and we believe this is a consequence of the noncentrosymmetric crystal structure. As a result the crystal produces a polarized beam of neutrons from an incident unpolarized beam. In resonant scattering experiments at the ID20 beamline of the ESRF the second-order magnetic satellite, which is a direct consequence of the cycloidal structure and the resonant cross section, was observed with the photon energy tuned to the uranium M_4 edge. The ratio of this to the first-order satellite is more than an order of magnitude less than that found in similar experiments on Ho. We have also observed weak resonant effects at the Pt L_3 and Ge K edges.

I. INTRODUCTION

The magnetic interactions that lead to ordered magnetic structures in the rare-earth metals and compounds are reasonably well understood, viz., a relatively weak direct interaction between the localized $4f$ electrons on adjacent sites, but a strong Ruderman-Kittle-Kasuya-Yosida (RKKY) indirect interaction passing through the itinerant $5d$-$6s$ states.[1] This interplay results in a panoply of magnetic configurations in which noncollinear arrangements of the magnetic moments tends to be the norm rather than the exception. In passing from the $4f$ to the $5f$ electrons as the principal unpaired states a number of important differences are evident. The greater spin-orbit coupling in the $5f$ systems as compared to their $4f$ counterparts leads to greater anisotropy and a higher preponderance of collinear structures. The energetics of noncollinear magnetic structures in $5f$ systems tends to favor multi-**q** arrangements.[2] In these magnetic structures the resultant magnetic moments tend to point along all equivalent axes of a special symmetry. Well-known examples are the cubic NaCl-type structures of compounds such as USb. This compound has magnetic Fourier components along each of the six $\langle 100 \rangle$ equivalent axes, so that the resultant moments are along $\langle 111 \rangle$.[2] This $3\mathbf{q}$ structure is, of course, noncollinear, but the aspect of noncollinearity is quite different from that found, for example, in the helix of holmium metal.

Much progress has been made in understanding the specifics of magnetic arrangements in uranium compounds by the work of Sandratskii and Kubler[3,4] who have used local-spin density functional theory and incorporated spin-orbit coupling to examine the stability of certain noncollinear magnetic arrangements. One of the points to emerge from this discussion is that helical type of magnetic arrangements are unlikely to be present in actinide materials as the spin-orbit interaction tends to align the moments along high-symmetry directions, and one of the aspects of a general helical structure is that the moments may point along any direction in the plane of the helix.

To our knowledge, there is only *one* system reported so far involving an actinide ion that has a helical magnetic structure. This is the ternary orthorhombic compound UPtGe, which was first reported to be antiferromagnetic ($T_N \sim 50$ K) from bulk measurements.[5] Interestingly, three independent reports involving neutron diffraction on the atomic and magnetic structure of UPtGe appeared simultaneously. The first study was that of Szytula *et al.*[6] who used

polycrystalline samples and reported the crystal structure as the TiNiSi type (*Pnma*, space group No. 62) and a cycloid magnetic structure with a moment of $1.1\mu_B$ per uranium. Also using polycrystalline samples, Robinson *et al.*[7] discussed whether the atomic structure was of the TiNiSi form, or the disordered analog of the $CeCu_2$ type (*Imma*, space group No. 74) and preferred the TiNiSi type. They established the ordered magnetic wave vector as $\boldsymbol{\tau}=[0,0.554(1),0]$ and suggested that the form of the cycloid was elliptical with the major axis ($1.41\mu_B$) in the direction parallel to $\boldsymbol{\tau}$ as compared to $1.02\mu_B$ perpendicular to $\boldsymbol{\tau}$. The third independent report on UPtGe was a conference paper from Kawamata *et al.*[8] that also reported a cycloid with $\sim 1\mu_B$ and $\boldsymbol{\tau}=[0,0.57,0]$. Our particular interest was in examining this cycloid in more detail, especially with the neutron polarimeter at the ILL, and also with synchrotron radiation using the technique of resonant x-ray magnetic scattering (RXMS).

II. CRYSTAL STRUCTURE

The single crystal used in this study was the same as used in Ref. 8 and was grown under argon using a tri-arc furnace. Its size is $\sim 4\times 3\times 5$ mm^3. The crystal structure is orthorhombic. In the TiNiSi (*Pnma*) notation the lengths of the axes are $a=7.17$ Å, $b=4.32$ Å, $c=7.50$ Å. Integrated neutron intensities were collected on both the D9 (hot source, $\lambda=0.84$ Å) and D15 (thermal source, $\lambda=1.172$ Å) four-circle diffractometers. A small piece of the crystal was also examined at the Institute for Transuranium Elements, Karlsruhe with a CAD four-circle diffractometer (Mo $K\alpha$ radiation, $\lambda=0.71$ Å). These extensive data sets showed that all $h+k+l=$ odd type of reflections were either very small, or zero. This excludes the space group *Pnma* of the TiNiSi structure, which all previous authors have assumed to be the correct crystal structure. Furthermore, a careful examination showed that $hk0$ reflections are present with h and k both odd. This excludes a glide plane perpendicular to **c**, and hence the space group *Imma* of the $CeCu_2$ structure. Moreover, refinements of both the x-ray and neutron data gave crystallographic *R* factors between 20 and 40 % for both the TiNiSi and $CeCu_2$ structures. UPtGe clearly does not have either of these crystal structures.

After considerable effort, we have found a reasonable fit to the structure type EuAuGe[9] (*Imm*2, space group No. 44). The results of the neutron and x-ray refinements are given in Table I. This space group has two important differences from those of the TiNiSi and $CeCu_2$ form. First, the space group is noncentrosymmetric, whereas the earlier two are centrosymmetric. Second, in the new space group there are *independent* positions for two uranium atoms. There is a change in the axes (interchanging **a** and **b**) in going from the *Pnma* to the *Imm*2 space groups, but this is simply confusing rather than fundamental. Projections of the two structures down the shortest axes are illustrated in Fig. 1. Note that to obtain the best fit with the sites fully occupied we have interchanged the Pt and Ge sites as compared to those given for Au and Ge in Ref. 9. The best *R* factor obtained with the Pt and Ge in the positions given by Ref. 10 is 9.5%, whereas it drops to 7.2% when these are interchanged. No improvement in the neutron or x-ray *R* factors was obtained by allowing disorder on the Pt and Ge sites, but it should be pointed out that for neutrons the scattering lengths are 8.185 and 9.60 fm for Ge and Pt, respectively, so the sensitivity to disorder is not substantial.

TABLE I. Results of least-squares fits of neutron (taken at $T=80$ K) and x ray (taken at RT) data to the structural parameters of the EuAuGe structure (*Imm*2, space group No. 44) with the axes defined as $a=4.32$ Å, $b=7.17$ Å, and $c=7.50$ Å. The position of U_1 is fixed in each refinement. Errors on other atomic coordinates are indicated on the least-significant digit. In the neutron (x ray) refinements a total of 278 (149) independent reflections were used.

Atom	Point symmetry symmetry	Position		Neutron	X-ray
U_1	$2a$ $mm2$	$(0,0,z)$	z	0.625	0.625
U_2	$2b$ $mm2$	$(0,1/2,z)$	z	0.686(1)	0.688(1)
Pt	$4d$ $m\cdots$	$(0,y,z)$	y	0.7217(5)	0.720(1)
			z	0.314(1)	0.328(1)
Ge	$4d$ $m\cdots$	$(0,y,z)$	y	0.2060(4)	0.221(2)
			z	0.984(1)	0.002(2)
R factors				7.2%	8.7%

Although we now have *R* factors of ~ 7 and 9 % for the neutrons and x rays, respectively (rather than 40% for the *Pnma* structure) we still have some concern that the structure of at least the Pt and Ge atoms may not be fully correct. First, neutron data of this quality usually refines to between 2–3 %. It is more difficult to be certain of the absorption corrections in the x-ray case with such heavy elements, but absorption for neutrons is negligible, as is extinction in the present case. Second, some of the refined temperature factors are negative. Thus we are left with some uncertainty in the exact crystal structure of UPtGe. We have tried, unsuccessfully, a number of other space groups. However, we should emphasize that with respect to the uranium atoms, which are the only ones carrying a magnetic moment, the configuration we propose is essentially the same as that already in the literature, and allows us to continue to discuss the physics of the magnetic interactions. We show in Fig. 2 the arrangement of U atoms projected down the shortest axis (**a** in the *Imm*2 structure). These can be thought of slightly buckled chains running through the structure parallel to **b** and placed

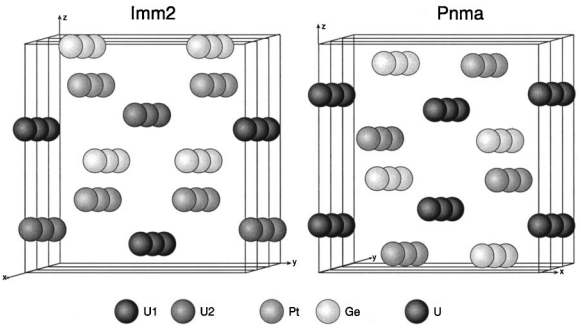

FIG. 1. The structures (left) *Imm*2 and (right) *Pnma*. Both are shown projected down the shortest axis. The different arrangement of Pt and Ge chains parallel to this short axis may be clearly seen in this projection.

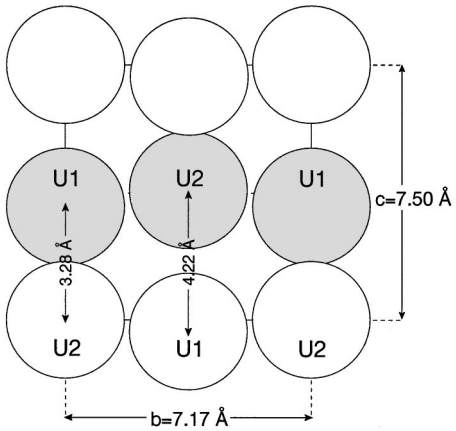

FIG. 2. Projection of the U atoms down the **a** axis of the $Imm2$ structure. The open and shaded atoms are separated by $a/2 = 2.16$ Å in the vertical direction. The circles have a diameter of 3.5 Å. The distances are those in the projection. To obtain the U_1-U_2 distances one must add to the values in the figure the $a/2$ displacement in quadrature, so that the distances become 3.93 and 4.74 Å, respectively. The U_1-U_2 distance almost parallel to the **b** axis is 3.61 Å.

at x coordinates of 0 and 1/2. The buckling of the chains here is shown to result in two U-U projections down the **a** axis of distances of 3.28 and 4.22 Å parallel to **c**. In the refinement of Robinson *et al.*[7] in the $Pnma$ space group the same projected distances are 3.24 and 4.26 Å. Fixing the x coordinate, which they refine to 0.0032(3), to zero, the arrangement of U atoms in the two space groups is almost identical. Because of the special positions of the U_1 and U_2 atoms in the $Imm2$ structure, they may be arranged in a centrosymmetric configuration (as shown in the figure) but the full space group is noncentrosymmetric. What is different between the two space groups is that the Pt and Ge atoms may also be placed on chains parallel to **b** in the $Imm2$ structure, whereas they alternate in the $Pnma$ space group [see Fig. 1(b)], and cannot be described in this way.

The nearest separation between U-U atoms is 3.61 Å, which far greater than the distance of ~3.2 Å at which strong $5f$-$5f$ overlap occurs. However, the U-Pt and U-Ge distances are between 3.0 and 3.2 Å so that hybridization between the U $5f$ and Pt $4d$ and Ge $4p$ states may be anticipated.

III. MAGNETIC STRUCTURE

A. Unpolarized neutrons

We initially used the D10 diffractometer ($\lambda = 2.36$ Å) to measure the positions and intensities of magnetic reflections at $T = 4.2$ K. These data established the magnetic wave vector $\boldsymbol{\tau} = [0.554(1),0,0]$, and we also measured the temperature dependence of the strong magnetic 0^+00 satellite. These results confirmed those in the literature, especially the work of Robinson *et al.*[7] Recall, again, that the **a** and **b** axes are interchanged in going from the $Pnma$ to $Imm2$ space groups. A fit was made to 156 integrated reflections giving the results in Table II. The propagation vector of the magnetic structure is along **a***, and the best fit to the intensity data suggests that the moments are in the **ac** plane. Initially,

TABLE II. Results for refinement of 156 magnetic reflections to a cycloidal model. The parameters are the magnitude of the uranium moments forming the envelope of the cycloid, and the phase relationship (ϕ) between U_1 and U_2. The ellipticity ε is defined as $\mu||[100]/\mu||[001]$. The R factor is a measure of agreement between the observed and calculated structure factors.

	$\mu\|\|[100]$ (μ_B)	$\mu\|\|[001]$ (μ_B)	ε	ϕ(deg.)	R factor
Model A					
$U_1 = U_2$	1.60(6)	1.28(5)	1.24(8)	10(2)	17%
Model B					
U_1	1.8(1)	1.5(1)	1.16(10)		
U_2	1.3(1)	0.9(1)	1.33(18)	0(5)	9%

in model A we have kept the moments on the two U sites identical. This gives an R factor of 17%, which is already quite good considering the complexity of the cycloid. However, the R factor may be significantly improved (to 9%) by allowing the moments on the two U sites to be different. We note that $\mu(U_1) > \mu(U_2)$, but that the ellipticity of both is close to the average value of 1.24. Both the average moment ($1.38\mu_B$) and ellipticity (1.24) are close to those of $1.22\mu_B$ and 1.39, respectively, found by Robinson *et al.*[7] The phase angle ϕ, which relates the propagation of the cycloid at U_1 compared to that at U_2, is close to zero. This is not surprising as the propagation direction is [100], and along this direction the atoms lie on fixed planes at $x = 0$ and 1/2, see Figs. 1 and 2. We searched for, but did not find, any evidence for second- or third-order satellites.

This is a cycloid structure, which is a special form of a helix, in which the angle between the normal to the plane of the moments and the propagation direction is $\pi/2$. When this angle is zero the helix is usually described as a spiral as found, for example, in Ho metal (and some other rare-earth systems). The reflection intensities alone may not lead to a unique model for the magnetic structure when it is noncollinear. For example, Robinson *et al.*[7] considered whether there might be a component out of the **ac** plane, or whether the configuration could be an amplitude-modulated wave, i.e., a collinear structure.

B. Polarized neutrons—the neutron polarimeter

1. General remarks and cross sections

Although our intensity data strongly support a cycloid, a less ambiguous result can be obtained by analyzing the polarization of the neutrons scattered into magnetic reflections. Zero-field neutron polarimetry was carried out using the spherical neutron polarimeter CRYOPAD II[10] installed on the sample table of the polarized-neutron triple-axis spectrometer IN20 at the ILL. We have recently discussed in detail the application of the polarimeter to the cycloidal magnetic structure in $DyFe_4Al_8$ (Ref. 11) and here we shall give only an abbreviated discussion relative to the experiments on UPtGe.

If we consider the case in which the magnetic and nuclear reflections are separated in reciprocal space (which is the case here for an incommensurate magnetic wave vector) then

it is relatively easy to get a qualitative understanding of how the polarimeter works by examining a few selected reflections. First, the polarization of the scattered neutrons will depend on the magnetic interaction vector—see Blume[12]—and its relation to the polarization of the incident neutrons. Following Ref. 10 we define this vector as **Q** (care should be taken not to confuse this use of **Q** with the more common use that associates this symbol with the scattering vector, which we shall call $\boldsymbol{\kappa}$)

$$\mathbf{Q}(\boldsymbol{\kappa}) = \hat{\boldsymbol{\kappa}} \times \left[\int \mathbf{M}(r) \exp(i\boldsymbol{\kappa}\cdot r) d^3r \right] \times \hat{\boldsymbol{\kappa}}$$
$$= \mathbf{M}(\boldsymbol{\kappa}) - [\mathbf{M}(\boldsymbol{\kappa})\cdot\hat{\boldsymbol{\kappa}}]\hat{\boldsymbol{\kappa}}, \quad (1)$$

where $\hat{\boldsymbol{\kappa}}$ is a unit vector in the direction of the scattering vector and $\mathbf{M}(\boldsymbol{\kappa})$ is a Fourier component of the magnetization. By definition **Q** lies in the plane perpendicular to $\boldsymbol{\kappa}$.

Turning now briefly to the description of the magnetic structure, it is well known that for an amplitude modulated wave the magnetic moment on the jth atom of the lth unit cell may be written

$$\mathbf{S}_{jl} = \mathbf{A}_j \cos(\boldsymbol{\tau}\cdot\mathbf{r}_l + \phi_j) \quad (2)$$

and for a helix or cycloidal magnetic structure

$$\mathbf{S}_{jl} = \mathbf{A}_j \cos(\boldsymbol{\tau}\cdot\mathbf{r}_l + \phi_j) + i\,\mathbf{B}j \sin(\boldsymbol{\tau}\cdot\mathbf{r}_l + \phi j), \quad (3)$$

where for the latter case $\mathbf{A}_j$ and $\mathbf{B}_j$ are perpendicular vectors giving the magnitude and direction of the major and minor axes of the elliptical envelope of the moment modulation on the jth atom, $\boldsymbol{\tau}$ is the propagation vector, and $\mathbf{r}_l$ the vector defining the origin of the lth unit cell. The phases of the modulation are given by ϕ_j.

To determine the precise form of **Q** it is necessary to substitute Eq. (2) or (3) into Eq. (1). However, there will be an important difference whether one is dealing with an amplitude modulated wave [Eq. (2)] or a helix [Eq. (3)] as in the former case **Q** and **Q*** will be parallel to each other, whereas in the latter they will not. The final point to remember is that when considering an incident direction of neutron polarization, components of **Q** that are parallel to it do *not* act on the neutron polarization (i.e., it is transmitted without change of polarization) whereas components that are perpendicular result in a precession of the neutron polarization.

For an amplitude modulated wave [Eq. (2)] the polarization ($\mathbf{P}_f$) of neutrons scattered by a pure magnetic reflection with $\mathbf{Q} \| \mathbf{Q}^*$ is related to the incident polarization ($\mathbf{P}_i$) by precession through π about the magnetic interaction vector **Q**. The situation is different when **Q** and **Q*** are not parallel (helix). In this case, if $\mathbf{P}_i$ is perpendicular to $\boldsymbol{\kappa}$ then the polarization is flipped around the longer component of **Q** and rotated towards the scattering vector by an angle which depends on the quantity $2\boldsymbol{\kappa}\cdot(\mathbf{A}\times\mathbf{B})/(\mathrm{A}^2+\mathrm{B}^2)$. One can see from this discussion that by measuring a few chosen reflections it is possible (i) to distinguish unambiguously whether the modulation is an amplitude modulated wave or a helix and (ii) that in the case of a helix the ellipticity can be determined with precision.

2. Experimental

To exploit the full capability of the neutron polarimeter it is necessary to place the plane in which the moments rotate (in this case the **ac** plane) *perpendicular* to the scattering plane. Since the scattering plane must contain the propagation direction (**a***), this requires the [001] plane vertical and the scattering plane containing [100] and [010]. For the h^+00 satellites the plane of **Q** and **Q*** is $[010]\times[001]$. The experimental observation is that neutrons incident along [001] and [100] are rotated in polarization, whereas those incident along [010] are left unchanged. This result is consistent with the moments having a component along [001] but *not* along [010]. (Naturally since the scattering vector is here placed along [100] no information is available about the moments in this direction.) Thus, from this one reflection (in fact we have examined a series of reflections along the $h00$ line) we can say that there is *no* magnetic component along the [010] axis. Considering other reflections of the form $h^{\pm}k0$, with $k \neq 0$, we show that there is also a component of the moment along [100].

3. Results

For a selection of $hk0$ reflections the direction of the scattered polarization was determined with the incident polarization successively parallel to the vertical direction (z), the scattering vector $\boldsymbol{\kappa}$ (x), and a third direction (y) that completes the right-handed Cartesian set. The final directions of polarization of the scattered neutrons may then be refined against a single parameter, the ellipticity (ratio of major to minor axes) of the cycloid. The results are given in Table III. The ellipticity at 4 K is 1.24(3) with the major axis parallel to [100], i.e., parallel to $\boldsymbol{\tau}$. This is in excellent agreement with the results of the refinement of the unpolarized-neutron data, giving confidence that the details of the magnetic structure are correct.

4. Discussion

Two further interesting points are worth making about the polarimeter results. First, the data cannot be used to extract values for the magnetic moments in the case in which the magnetic and nuclear reflections are separated (as is the case here). To do this one must measure intensities and normalize with the nuclear reflections, as done in the refinement of the unpolarized neutron data (Table II). The second point goes back to the original paper by Blume,[12] who noted that in the special case of a single chirality spiral, unpolarized incident neutrons will be scattered to produce a single polarization state. This is because of a term $i(\mathbf{Q}^*\times\mathbf{Q})$ in the cross section for the scattered neutrons. For a right-handed helix this has a nonzero component along the scattering vector. For a left-handed helix its sign is changed. Thus in a normal crystal, in which both right- and left-handed helices are equally likely, the net result is zero polarization of the scattered neutrons. Small effects were observed in materials such as MnP,[13] for example, and in most centrosymmetric samples these effects appear to be small as observed either with neutrons[14] or x rays,[15] but very large effects—indicating almost a single chirality—are known to exist in materials that are noncentrosymmetric, such as MnSi.[16] Indeed, Bak and Jensen[17] have emphasized that the noncentrosymmetric nature of the

TABLE III. CRYOPAD polarimetric data for the first-order satellites in UPtGe. P_i and P_f are the polarization vectors of the incident and scattered beams. The polarization axes are $x||\boldsymbol{\kappa}$, y is in the scattering plane, $[100]\times[010]$, perpendicular to $\boldsymbol{\kappa}$, and z is vertical and parallel to [001]. P_c is the calculated polarization from the magnetic structure model. The estimated error bars on P_i and P_f are 0.01 and 0.03, respectively. The agreement R factor $=14\%$.

	P_i			P_f			P_c		
hkl	x	y	z	x	y	z	x	y	z
0^+00	0.00	0.00	0.90	0.01	−0.05	0.91	0.00	0.00	0.90
	0.00	0.90	0.00	0.08	−0.91	−0.04	0.00	−0.90	0.00
0^+20	0.00	0.00	0.90	0.94	−0.11	−0.12	0.97	0.00	−0.11
	0.00	0.90	0.00	0.94	−0.02	0.03	0.97	0.11	0.00
2^-20	0.00	0.00	0.90	−0.91	0.00	0.16	−0.95	0.00	0.20
	0.00	0.90	0.00	−0.91	−0.10	−0.01	−0.95	−0.20	0.00
0^-20	0.00	0.00	0.90	−0.93	0.05	−0.14	−0.97	0.00	−0.11
	0.00	0.90	0.00	−0.92	0.13	−0.02	−0.97	0.11	0.00
	0.00	0.00	−0.90	−0.92	0.14	0.09	−0.97	0.00	0.11
	0.00	−0.90	0.00	−0.93	0.00	−0.04	−0.97	−0.11	0.00
2^+20	0.00	0.00	0.90	0.78	−0.12	0.35	0.81	0.00	0.51
	0.00	0.90	0.00	0.85	−0.38	−0.02	0.81	−0.51	0.00
	0.00	0.00	−0.90	0.84	0.03	−0.37	0.81	0.00	−0.51
	0.00	−0.90	0.00	0.80	0.41	0.06	0.81	0.51	0.00
0^+20	0.00	0.00	0.90	0.92	−0.17	−0.13	0.97	0.00	−0.11
	0.00	0.90	0.00	0.93	−0.08	0.00	0.97	0.11	0.00
	0.00	0.00	−0.90	0.91	−0.18	0.15	0.97	0.00	0.11
	0.00	−0.90	0.00	0.91	−0.30	0.02	0.97	−0.11	0.00

underlying lattice is central to understanding the possibility of a large chirality effect. Our experiments on the UPtGe crystal established that there was *no* depolarization of the scattered neutrons in any Bragg reflection. Depolarization signifies domains (or mixed chirality in the case of a spiral). Thus, our crystal transformed into a *single* magnetic domain. Repeated heating above T_N and cooling did not change the domain configuration. This was demonstrated unequivocally by the observation that the direction of the polarization of the neutrons scattered by the 0^+20 reflection was almost parallel to the scattering vector regardless of the direction of the incident polarization.

It should be noted that a cycloidal structure does not have an *absolute* chirality since the sense of a cycloid is reversed by rotation of π about its propagation direction. The apparent chirality of the structure is therefore reversed by this rotation and will appear to be opposite for the h^+kl and h^-kl reflections. Since this is a real rotation one can perform on the crystal it is clear that the ''chirality'' of the cycloid cannot exist. Changing chirality requires an improper rotation, i.e., one that involves the use of a mirror plane, in the sense that the left hand may be transformed into the right. As discussed earlier, the cycloid is a special case of the helix, but with the angle between the normal to the plane of the moments and the propagation direction equal to $\pi/2$. Any deviation of this angle from $\pi/2$ allows one to talk of chiral domains, but the domains in UPtGe do not have that character. Nevertheless, it seems likely that the formation of a single domain in the case of UPtGe is related to the noncentrosymmetric nature of the crystal structure. It should also be noted that the rotation of π about **a**, which relates the two cycloidal domains also reverses the direction of the **c** axis, which is a *polar* twofold axis in $Imm2$.

IV. SYNCHROTRON X-RAY EXPERIMENTS

A. General remarks and cross sections

As stated in the Introduction, one of the original motivations for the experiments on the UPtGe crystal was that with a cycloid structure a new series of magnetic satellites with periodicity 2τ should be observed when the x-ray photon energy coincides with the resonance condition. Resonant x-ray magnetic scattering (RXMS) is now becoming a common technique and we refer the reader to a number of papers, in particular, the work of Hill and McMorrow,[18] which summarizes in an excellent way the terms in the scattering cross section. In the case of actinide materials, the important resonance involves transitions from the $3d$ to $5f$ states, i.e., the M_4 and M_5 edges. The resonant enhancement at these edges is very considerable,[19,20] so that the scattering may readily be observed. To understand the scattering cross section in the resonant condition we repeat briefly the formula given in Ref. 18,

$$f_{nE1}{}^{\mathrm{RXMS}}=[(\hat{\boldsymbol{\varepsilon}}'\cdot\hat{\boldsymbol{\varepsilon}})F^{(0)}-i(\hat{\boldsymbol{\varepsilon}}'\times\hat{\boldsymbol{\varepsilon}})\cdot\hat{\mathbf{z}}_nF^{(1)} +(\hat{\boldsymbol{\varepsilon}}'\cdot\hat{\mathbf{z}}_n)(\hat{\boldsymbol{\varepsilon}}\cdot\hat{\mathbf{z}}_n)F^{(2)}], \tag{4}$$

where the scattering involves an electric dipole transition (E1) between the $3d$ and $5f$ shell and $\hat{\boldsymbol{\varepsilon}}$ and $\hat{\boldsymbol{\varepsilon}}'$ are unit vectors in the directions of the incident and scattered polarization vectors, respectively, and $\mathbf{k_i}$ and $\mathbf{k_f}$ are the incident and scattered wave vectors, respectively. $\boldsymbol{\kappa}=\mathbf{k_f}-\mathbf{k_i}$ is the wave vector transfer. The terms $\hat{\mathbf{z}}_n$ represent a unit vector in the direction of the magnetic moment of the nth atom. The first term of Eq. (4) simply contributes to the charge peak, since it contains no dependence on the magnetic moment. In

an incommensurate antiferromagnet (as UPtGe) the second term produces first harmonic (i.e., at the positions τ) magnetic satellites, and the third term, which contains two powers of the magnetic moment, produces second-order harmonics at the positions 2τ. We stress that these satellites are intrinsic to the resonant process; they do not signify a modulation of the magnetic modulation, which can also give rise to higher-order satellites. The amplitudes of these various terms are governed by the factors $F^{(i)}$ which are determined by the nature of the resonance, the probability of the transitions, the amount of overlap between the states involved, and the nature of the decay channels. Normally we expect $F^{(2)} < F^{(1)}$. If we can observe first- and second-order satellites then it should be possible to determine the ratio $F^{(1)}/F^{(2)}$. To our knowledge these have not been calculated for the actinides, although this would seem possible in an *atomic* picture as some calculations exist for the rare earths.[21] Whether, of course, such calculations are relevant to experiments in actinides, in which the atomic picture of localized *f* electrons often fails, is another question. Recognizing these uncertainties our goal is more modest, being to measure experimentally the ratio of $F^{(1)}/F^{(2)}$ in UPtGe, and compare this ratio with the value found for holmium.[22]

Hill and McMorrow[18] have reduced the above cross section to a more tractable form. Since our experiments have been done with σ polarization of the photons incident on the crystal, we need only retain the terms corresponding to $\sigma \rightarrow \sigma$ and $\sigma \rightarrow \pi$ cross sections. For these experiments we have not used polarization analysis at the uranium M_4 edge, so the photons arriving at the detector will be the sum of these two channels. Furthermore, since the dipole transitions are much stronger in the actinides[19,20] than the quadrupole transitions, which have not yet been observed, we retain only the dipole terms. If θ is the Bragg angle the terms of interest are

$$I\{F^{(1)}\} \propto |[z_3 \sin\theta - z_1 \cos\theta]|^2, \quad \text{all in the } \sigma \rightarrow \pi \text{ channel,}$$

$$I\{F^{(2)}\} \propto |[z_2{}^2]|^2 \quad \text{in } \sigma \rightarrow \sigma, \tag{5}$$

$$I\{F^{(2)}\} \propto |[z_2(z_1 \sin\theta + z_3 \cos\theta)]|^2 \quad \text{in } \sigma \rightarrow \pi.$$

The terms z_1, z_2, and z_3 are components of a unit vector along the direction of the magnetic moment, such that z_3 is the component along the scattering vector $\boldsymbol{\kappa}$ (defined by $\mathbf{k_i} - \mathbf{k_f}$), z_1 is the component in the scattering plane perpendicular to $\boldsymbol{\kappa}$ (defined by $\mathbf{k_i} + \mathbf{k_f}$), and z_2 is the component perpendicular to the scattering plane (defined by $-\mathbf{k_i} \times \mathbf{k_f}$). In the experiment the scattering plane is $[100] \times [010]$. These expressions have to be evaluated with the correct substitution of the z_i and then summed over all atoms in the unit cell in the usual way, see Ref. 18. From the expressions for the terms in $F^{(2)}$ two general points emerge if a second-order satellite is to be observed: (i) there must be a component z_2 *out of the scattering plane*, (ii) the magnetic structure must be *noncollinear*, except in the case in which only a z_2 component exists and then there will be no signal at τ, so this situation does not help in determining their intensity ratio.

We recall from our earlier discussion of the magnetic structure of UPtGe that the magnetic structure is established by the neutron polarimeter to be a cycloid in the **ac** plane. By orienting the crystal so that the scattering plane contains the vectors **a*** and **b*** we have fulfilled the conditions to observe a second-order satellite as the moments have components in the **c*** direction, which is perpendicular to the scattering plane. We have found the strongest signal at the position $0^{2+}00$ so that the scattering vector is along [100], and z_1 along the [010] direction is zero. The term in $\sigma \rightarrow \pi$ in Eq. (5) concerning $F^{(2)}$ then reduces to $z_2 z_3 \cos\theta$.

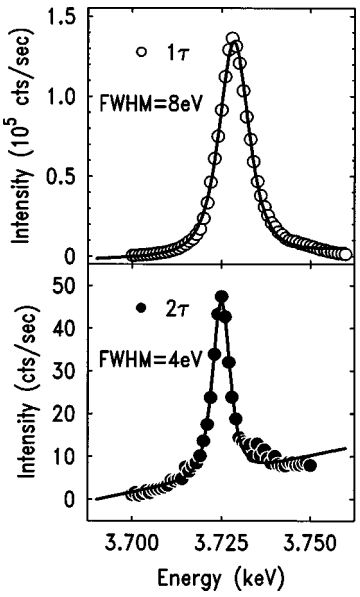

FIG. 3. Intensity as a function of incident photon energy of the first- and second-order satellites, 2^-00 and $0^{2+}00$, respectively. Notice the different energy widths of the two satellites.

B. Experimental method and results

The experiments were performed on the ID20 undulator beamline[23] of the European Synchrotron Radiation Facility, Grenoble, France. A double crystal, Si(111), monochromator selects the appropriate x-ray energy and harmonics of higher incident energy are eliminated by the use of silicon mirrors. The use of a closed-cycle refrigerator limited the base temperature to ~ 9 K. Exactly the same crystal as used for neutron experiments was used for the x-ray studies. The (010) face was polished using standard techniques to give a mirror finish. No further annealing was performed. The mosaic of the crystal (full width at half maximum) is about 0.2° which is adequate for neutrons, but rather large for x-ray studies. As is standard practice, at each photon energy the photon beam was moved around on the surface to find the best place at which to perform the experiments.

Figure 3 shows an energy scan through the 2^-00 (first-order) and $0^{2+}00$ (second-order) satellites at $T = 10$ K. Both peaks show resonant behavior confirming that they are magnetic and neither is present above T_N. Their widths in energy space are quite different, with the second-order satellite being much narrower than the first-order one. The first-order satellites have a width in momentum space indistinguishable from that of the charge peaks. On the other hand, the second-order and third-order (see below) satellites have a width in the longitudinal directions (i.e., parallel to $\boldsymbol{\tau}$) that is significantly larger (by $\sim 50\%$) than the first-order one. The widths in the transverse directions appear to be the same.

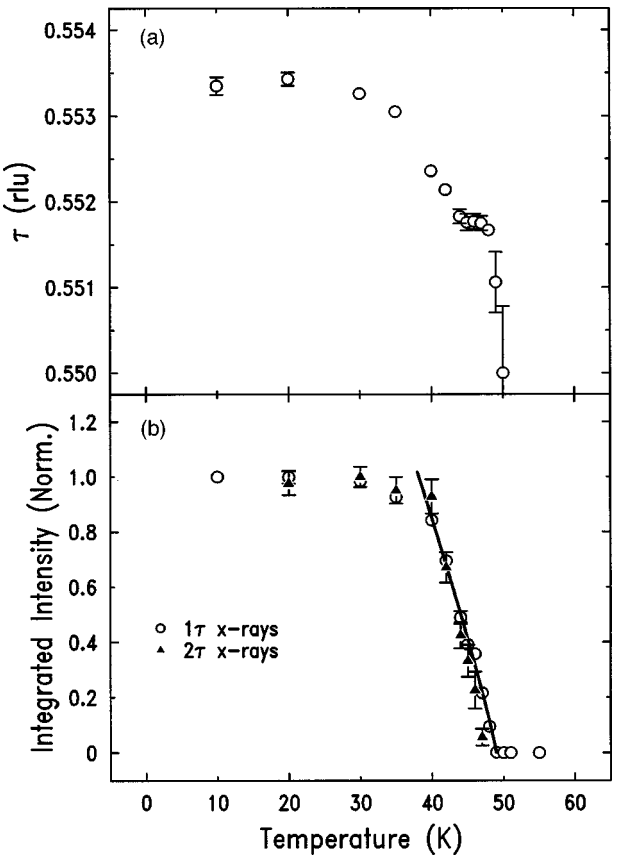

FIG. 4. (a) Variation of the modulation wave vector τ as a function of temperature as measured in the x-ray experiment. (b) Dependence of the intensities of the first- and second-order satellites as a function of temperature as measured in the x-ray experiment. The solid line shows the function $I \propto (t^{2\beta})^2$ as discussed in the text, with β taken from the first-order satellite.

Figure 4 shows the temperature dependence of the modulation vector τ and the first- and second-order satellites. Other 2τ satellites were also observed, all about the same level of intensity. Conventionally, the first-order satellite has a temperature dependence given by $I(\tau) \propto (t^{\beta})^2$, where $t = (T_N - T)/T_N$ and β is the critical exponent. As shown in Fig. 4, within our statistics the temperature dependence of the second-order satellite also follows $I(2\tau) \propto (t^{\beta})^2$, whereas conventionally the temperature dependence should follow $(t^{2\beta})^2$. This was the case for the second-order satellite in holmium,[24] but with our limited statistics due to the weakness of our signal, we cannot be sure this difference is significant. The satellite is absent above T_N, as expected. Note that this satellite intensity is dependent on the ellipticity [see Eq. (6) below] and we have not measured how this changes as a function of temperature.

Returning now to our original aim, we can determine the ratio of the terms $F^{(2)}/F^{(1)}$. Following the example No. 3.1 given in Ref. 18 we determine the expression for a cycloid with ellipticity ε, where this is defined (as above) as the ratio of the amplitude of the cycloid envelope parallel to the propagation vector divided by that perpendicular. The plane of the cycloid is perpendicular to the scattering plane. The final expression after some algebra is

$$I(\tau)/I(2\tau) = (2F^{(1)}/F^{(2)})^2 \varepsilon^2 \left[\frac{\sin^2 \theta_1}{\varepsilon^{-2} + \cos^2 \theta_2} \right], \qquad (6)$$

where the first-order satellite occurs at a Bragg angle of θ_1 and the second-order one at θ_2. The intensities $I(\tau)$ and $I(2\tau)$ are integrated over both the longitudinal and transverse directions and corrected for the appropriate Lorentz factors. Note that this expression has the limits previously discussed. Since ε is the ratio of the moment amplitude parallel to τ to that perpendicular to it in the plane of the cycloid, it can be thought of as the amplitude ratio of moments along z_3 compared to those along z_2 in the notation of Eq. (5). As $\varepsilon \to \infty$ the moments lie totally along τ (z_3) so that $I(2\tau) \to 0$. On the other hand, as $\varepsilon \to 0$ then the moments are along z_2 and $I(\tau) \to 0$. We observe $I(\tau)/I(2\tau) \sim 5 \times 10^3$, and with $\varepsilon = 1.3$ as defined by the neutron polarimeter we have $F^{(1)}/F^{(2)} \sim 60$.

This is to be compared to a ratio of ~ 2.7 in holmium.[18] In other words, the intrinsic second-order satellite in this uranium compound is some $(30)^2$, i.e., 900 times weaker than that observed in holmium.

A further point of interest (see Fig. 3) is that the second-order satellite is much narrower in energy space than the first-order satellite. The fact that it is narrower in the case of the second-order satellite could arise from the fact that the $F^{(1)}$ and $F^{(2)}$ terms contain different overlap integrals between the two states[18] so that their energy widths may be different. The energy resolution in the case of ID20 is about 0.5 eV. This will be a further test for theory when these cross sections are calculated.

C. General characterization of magnetic modulation

The intensity at the M_4 resonance of uranium is so strong (1.25×10^5 cts/sec. at 200 mA synchrotron current) that the probe may be used not only to investigate details of the cross section, as discussed above in connection with the second-order satellite, but also to investigate details of the magnetic structure which are impossible, or at least difficult, with neutrons. We have already shown the temperature dependence of the wave vector in Fig. 4. In this case it is not so much the intensity of the M_4 resonance that is important but the resolution available. In addition, we have observed third-order satellites in the x-ray study which have an energy dependence similar to the first-order magnetic satellites. The intensity of the $0^{3+}00$ satellite is ~ 60 cts/s compared to the first-order satellite intensity of 1.2×10^5 cts/s so that the intensity of the third and first order is $\sim 5 \times 10^{-4}$. This ratio is below the sensitivity of the neutron experiment on D10. The observation of this satellite shows that the magnetic structure is not a pure cycloid at the lowest temperature, but there is some distortion of the wave form. However, the distortion is small, and does not substantially affect the conclusions drawn from the neutron experiments. Interestingly, the energy widths of the third-order satellite are very comparable to those of the first-order satellite. This reinforces our arguments about the narrow width of the second-order satellites arising from the $F^{(2)}$ term, as both the first- and third-order satellites depend on the $F^{(1)}$ term in the cross section of Eq. (4).

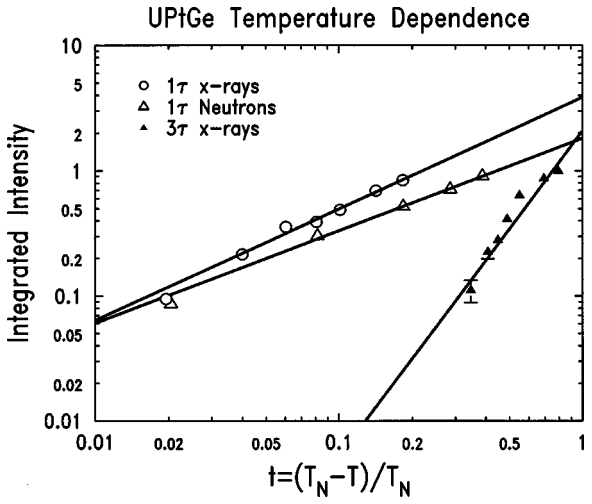

FIG. 5. T dependence of first- and third-order satellite from x rays and first-order satellite from neutrons. The slopes give $I(\tau)_{\text{x rays}}=0.44(4)$; $I(\tau)_{\text{neutrons}}=0.37(3)$; $I(3\tau)_{\text{x rays}}=1.30(8)$. $T_N=48.9(1)$ K.

The temperature dependence of the first- and third-order satellites are shown as a function of reduced temperature in Fig. 5. Also shown are the intensities determined with neutrons at D10. The value of $T_N=48.9(3)$ K, which is consistent with the value of ~ 51 K determined with a polycrystalline sample.[7] The values of β are first-order neutrons $-0.44(4)$, first-order x rays $-0.37(3)$, third-order x rays $-1.30(8)$. The results for the first order are consistent with both techniques and, again as expected, $\beta(3\tau)\sim 3\beta(\tau)$. The widths in momentum space of the satellites reflect Fourier harmonics of the cycloid, and it is normal that the higher order harmonics are wider since they are more sensitive to ''faults'' in the exact cycloid arrangement.

At higher energies, see below, we have also observed a weak *charge* 2τ satellite, this was identified as such because for these measurements we used an analyzer to determine the polarization state of the scattered photons. The signal appeared only in the $\sigma\rightarrow\sigma$ channel. The presence of such a charge modulation is not surprising as it represents a magnetoelastic coupling between the uranium magnetic moments and the lattice. It is thus a magnetically induced charge density wave accompanying the cycloid. Such a modulation has a structure factor that depends on the uranium structure factor, but it will also increase as $|\boldsymbol{\kappa}|^2$ so is difficult to observe at low angles. We have observed scattering at the $6^{-2}00$ and $5^{-2}10$ positions with photons of incident energy 11.05 keV. Such positions in reciprocal space cannot be examined at the U M_4 edge (3.728 keV) as the scattering conditions cannot be satisfied. Furthermore, the penetration of higher-energy photons greatly increases the effective scattering volume, so it is not surprising that the *charge* contribution at the 2τ position is seen only at higher energies and higher scattering angles.

D. Resonant intensity at edges of nonmagnetic elements

Recently, it has been observed[25] that very large resonant intensities are observed at the K edges of Ga and As in the antiferromagnetic compounds UGa_3 and UAs. In the present experiment we searched for effects associated with both the Pt and Ge edges in UPtGe. These energies are above 11 keV and because of the strong fluorescence it is necessary to use an analyzer to suppress the background. We used a Al(333) analyzer, which scatters at 90° for an energy of 11.248 keV.

We show in Fig. 6 the results at the U M_4, Ge K, and Pt L_3 edges, respectively. The enhancements to the nonresonant magnetic scattering at the Ge and Pt edges are relatively small, and of an amplitude to be expected given that there will be some hybridization between the U $5f$ states and both the Ge $4p$ and the Pt $6d$. Note that quite large signals were observed[26] at the Pt L_3 edge in the alloy CoPt, so the polarization of the $6d$ band of Pt in UPtGe also is not surprising. Normally, one would not anticipate observing a polarization of the $4p$ band of Ge, so such a polarization probably occurs via their hybridization with the U $5f$ electrons. Note that a signal could also occur if the spatial extent of the spin-up $4p$ states is different from that of the spin-down $4p$ states, without any net polarization.

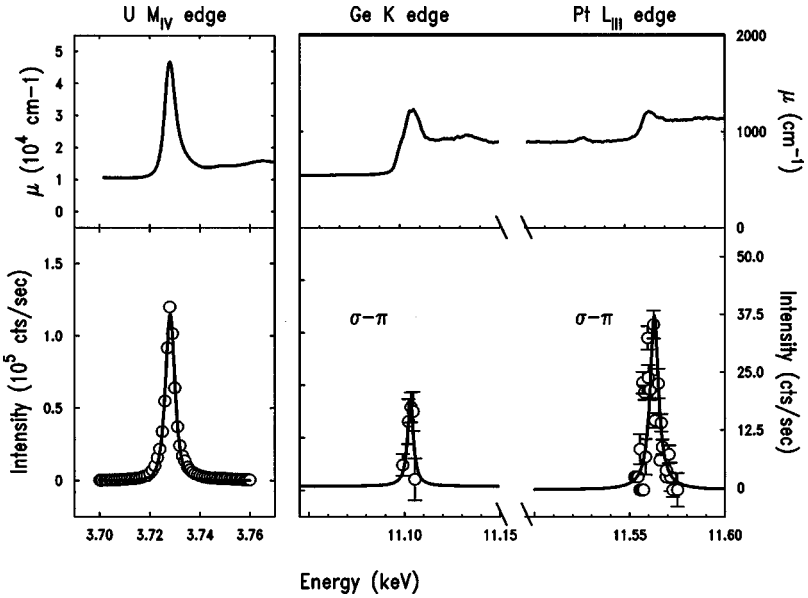

FIG. 6. Upper panels: absorption as a function of energy as derived from the fluorescence data. Lower panels: resonant enhancements at the U M_4, Ge K, and Pt L_3 edge as a function of energy across the edges. Note that polarization analysis was used for the Ge and Pt edges so to compare relative intensities, those at the Ge and Pt should be multiplied by ~ 20 to account for the reflectivity of the analyzer Al(333).

V. CONCLUSIONS

Originally, this study was started to try and observe the 2τ magnetic satellite associated with the resonant process in x-ray scattering from a noncollinear magnetic structure. This effect has been reported for holmium but not for any actinide. The original experiments, at the X22C beamline of the NSLS at Brookhaven National Laboratory, were unsuccessful. This led us to question whether the reported *magnetic* structure of UPtGe was wrong, and perhaps was collinear, in which case the 2τ magnetic satellite would be absent. This, in turn, led to experiments with the neutron polarimeter at the ILL. These established that the magnetic structure was indeed a cycloid, close to what was reported in the literature, but a measurement of integrated intensities using unpolarized neutrons established that the *crystal* structure assigned to this compound was wrong. After solving this structure (Table I), we returned with the higher intensity (compared to X22C at NSLS) of the ID20 beamline, and indeed have observed the 2τ magnetic satellite with RXMS (Fig. 3). Its ratio compared to the first-order satellite in amplitude is more than an order of magnitude less than that observed in holmium. Hopefully, this, together with the possibility of measuring this ratio in other actinide compounds, will encourage theoretical calculations. Such calculations will help in further characterizing the *M* resonances, which are very large, and frequently used to investigate magnetic properties, especially of actinides.[20,27,28] The aim, of course, is to establish a relationship between the intensity of the RXMS scattering at the *M* edges and the magnitude of the ordered moments.

A careful analysis of the unpolarized data shows that the two independent uranium atoms in the crystal structure carry different magnetic moments (Table II), although the ellipticity of the cycloid envelopes at each site are similar. The Pt configuration around these two U sites is different, the average U-Pt bond being 3.04 Å for U_1 and 3.14 Å for U_2. We find $\mu(U_1) > \mu(U_2)$. Recently, in a study[29] of the site susceptibilities of the compound U_2Pt_2In, large differences were found between the susceptibilities at two independent U sites. Direct comparisons between these structures are, of course, difficult but these different moments in UPtGe illustrate the importance, and complexity, of hybridization between the U $5f$ and Pt $6d$ states.

Our experiments demonstrate the power not only of using single crystals, which is well known, but also in making both neutron and synchrotron measurements on the same crystal. This is especially true when the magnetic properties are as unusual as those in UPtGe. An interesting feature which emerges is that the crystal is a single antiferromagnetic domain below T_N, as established by the neutron polarimeter experiments. We believe this is associated with the noncentrosymmetric nature of the crystal structure.

We have measured weak polarization effects at both the Pt L_3 and Ge *K* edges. Signals have been previously seen at the Pt *L* edges,[26] but not, to our knowledge, at the Ge *K* edges. However, compared with recent experiments on UGa_3 and UAs (Ref. 25) the signal found in UPtGe is relatively weak, for example, its intensity is less than 5% of that found at the *K* edge of Ga in UGa_3 below T_N.

ACKNOWLEDGMENTS

We thank Robert Troc for giving us some ideas that led to the solving of the crystal structure, Nick Bernhoeft for discussions about the satellite widths, Leonid Sandratskii for his interest and encouragement to complete this project, and Gary McIntyre for some beam time on the D10 diffractometer. D.M. and S.C. acknowledge support from the TMR program of the European Community.

*Also at the European Synchrotron Radiation Facility, B.P. 220X, F-38043 Grenoble, France.

†Present address: Rutherford Appleton Laboratory, ISIS Facility, Chilton, Didcot, Oxon OX11 0QX, United Kingdom.

[1] J. Jensen and A. Mackintosh, *Rare-Earth Magnetism* (Clarendon Press, Oxford, 1991).

[2] J. Rossat-Mignod, G. H. Lander, and P. Burlet, in *Handbook of the Physics and Chemistry of the Actinides*, edited by A. J. Freeman and G. H. Lander (Elsevier Science, Amsterdam, 1984), Vol. 1, pp 415–515.

[3] L. M. Sandratskii and J. Kübler, Phys. Rev. Lett. **75**, 946 (1995).

[4] L. M. Sandratskii, Adv. Phys. **47**, 91 (1998).

[5] R. Troc and V. H. Tran, J. Magn. Magn. Mater. **73**, 389 (1988).

[6] A. Szytula, M. Kolenda, R. Troc, V. H. Tran, M. Bonnet, and J. Rossat-Mignod, Solid State Commun. **81**, 481 (1992). The authors of Ref. 6 refer to a spiral structure but this is incorrect. Both the spiral and cycloid are forms of helices. In the case of a spiral the angle between the propagation direction and the normal to the plane in which the moments turn is zero; in the case of a cycloid this angle is $\pi/2$. Figure 2 of their paper indicates that they mean a cycloid.

[7] R. A. Robinson, A. C. Lawson, J. W. Lynn, and K. H. J. Buschow, Phys. Rev. B **47**, 6138 (1993).

[8] S. Kawamata, K. Ishimoto, Y. Yanaguchi, and T. Komatsubara, J. Magn. Magn. Mater. **104-107**, 51 (1992).

[9] R. Pöttgen, J. Mater. Chem. **5**, 505 (1995).

[10] P. J. Brown, J. B. Forsyth, and F. Tasset, Proc. R. Soc. London, Ser. A **442**, 147 (1993).

[11] J. A. Paixão, M. Ramos Silva, S. Aa. Sørensen, B. Lebech, G. H. Lander, P. J. Brown, S. Langridge, E. Talik, and A. P. Goncalves, Phys. Rev. B **61**, 6176 (2000).

[12] M. Blume, Phys. Rev. **130**, 1670 (1963).

[13] G. P. Felcher, G. H. Lander, and T. O. Brun, J. Phys. (Paris), **32**, C1-577 (1971).

[14] V. I. Fedorov, A. G. Gukasov, V. Kozlov, S. V. Maleyev, V. P. Plakhty, and I. A. Zobkalo, Phys. Lett. A **224**, 372 (1997).

[15] C. Sutter, G. Grübel, C. Vettier, F. de Bergevin, A. Stunault, D. Gibbs, and C. Giles, Phys. Rev. B **55**, 954 (1997).

[16] M. Ishida, Y. Endoh, S. Mitsuda, Y. Ishikawa, and M. Tanaka, J. Phys. Soc. Jpn. **54**, 2975 (1985).

[17] P. Bak and M. H. Jensen, J. Phys. C **13**, L881 (1980); M. L. Plumer and M. B. Walker, *ibid.* **14**, 4689 (1981).

[18] J. P. Hill and D. F. McMorrow, Acta. Crystallogr., Sect. A: Found Crystallogr. **A52**, 236 (1996).

[19] D. B. McWhan, C. Vettier, E. D. Isaacs, G. E. Ice, D. P. Siddons, J. B. Hastings, C. Peters, and O. Vogt, Phys. Rev. B **42**, 6007 (1990); G. H. Lander, J. Alloys Compd. **250**, 544 (1997).

[20] E. Lidström, D. Mannix, A. Hiess, J. Rebizant, F. Wastin, G. H. Lander, I. Marri, P. Carra, C. Vettier, and M. J. Longfield, Phys. Rev. B **61**, 1375 (2000).

[21] M. Hamrick, Ph.D. thesis, Rice University, Houston, 1994.
[22] D. Gibbs, G. Grübel, D. R. Harshman, E. D. Isaacs, D. B. McWhan, D. Mills, and C. Vettier, Phys. Rev. B **43**, 5663 (1991).
[23] A. Stunault, C. Vettier, F. de Bergevin, N. Bernhoeft, V. Fernandez, S. Langridge, E. Lidström, J. E. Lorenzo-Diaz, D. Wermeille, L. Chabert, and R. Chagnon, J. Synchrotron Radiat. **5**, 1010 (1998).
[24] G. Helgesen, J. P. Hill, T. R. Thurston, D. Gibbs, J. Kwo, and M. Hong, Phys. Rev. B **50**, 2990 (1994).
[25] D. Mannix *et al.* (unpublished).
[26] F. de Bergevin, M. Brunel, R. M. Galera, C. Vettier, E. Elkaim, M. Bessiere, and S. Lefebvre, Phys. Rev. B **46**, 10 772 (1992).
[27] E. D. Isaacs, P. Zschak, C. L. Broholm, C. Burns, G. Aeppli, A. P. Ramirez, T. T. M. Palstra, R. W. Erwin, N. Stücheli, and E. Bucher, Phys. Rev. Lett. **75**, 1178 (1995).
[28] D. Mannix, G. H. Lander, J. Rebizant, R. Caciuffo, N. Bernhoeft, E. Lidström, and C. Vettier, Phys. Rev. B **60**, 15 187 (1999).
[29] A. Martin-Martin, L. C. J. Pereira, G. H. Lander, J. Rebizant, F. Wastin, J. C. Spirlet, P. Dervenagas, and P. J. Brown, Phys. Rev. B **59**, 11 818 (1999).